Role of particle size and surface functionalisation on the flexibility behaviour of switchable metal-organic framework DUT-8(Ni)

Supporting Information

Megan J. Thompson[¶], Claire L. Hobday[¶,†], Irena Senkovska[#], Volodymyr Bon[#], Sebastian Ehrling[#], Mariia Maliuta[#], Stefan Kaskel[#], Tina Düren[*,¶]

[¶] Centre for Advanced Separations Engineering, Department of Chemical Engineering, University of Bath, BA2 7AY, UK

[†] Current address: EaStChem School of Chemistry and Centre for Science at Extreme Conditions, University of Edinburgh, David Brewster Road, Joseph Black Building, Edinburgh, EH9 3FJ, UK

[#] Chair of Inorganic Chemistry, Department of Chemistry and Food Chemistry, TU Dresden, Bergstraße 66, 01069 Dresden, Germany

AUTHOR INFORMATION

* Prof. T. Düren, Centre for Advanced Separations Engineering, Department of Chemical Engineering, University of Bath, BA2 7AY, UK

E-mail: t.duren@bath.ac.uk

Section S1. Crystal morphology prediction

Bravais-Friedel-Donnay-Harker calculations were performed in Mercury to determine the equilibrium structures of DUT-8(Ni) (*op*) and DUT-8(Ni) (*cp*) [1, 2]. The CCCD number for the structures are 1056823 and 1034317 [3]). From this, the most dominant crystallographic planes could be determined to make the surfaces of the nanoparticle models. **Figure S1** shows the resulting structures and relative surface areas that are inversely proportional to the growth rate of each Miller Plane.

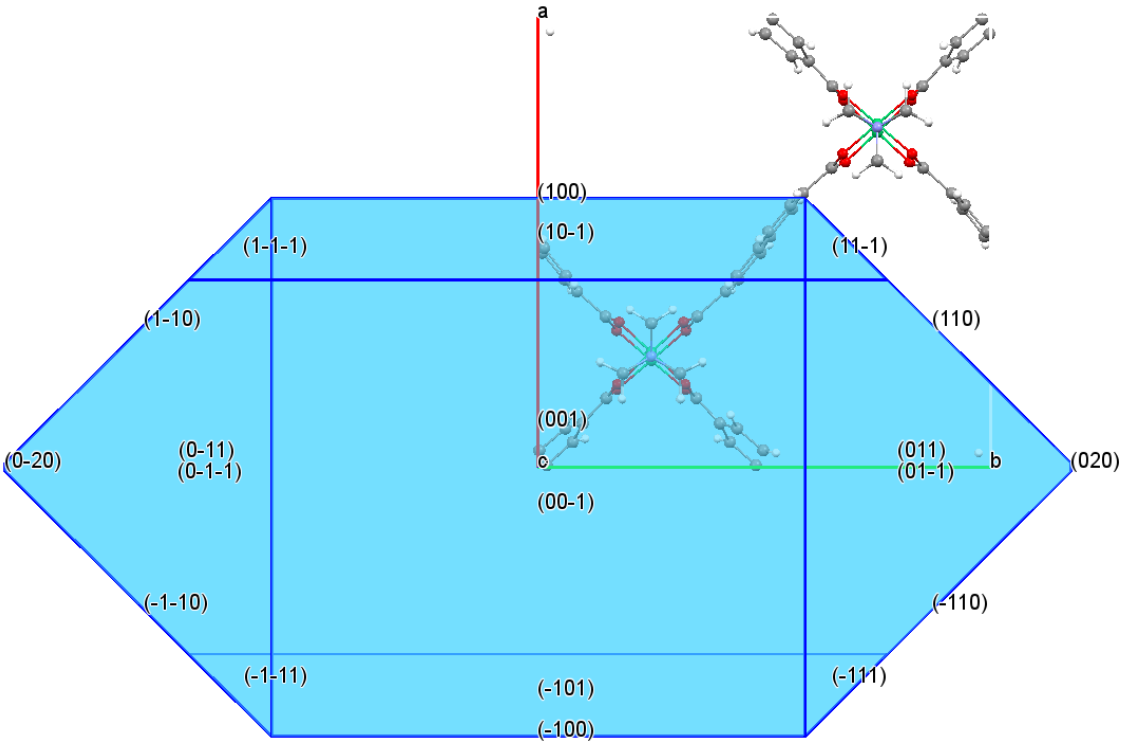

b)

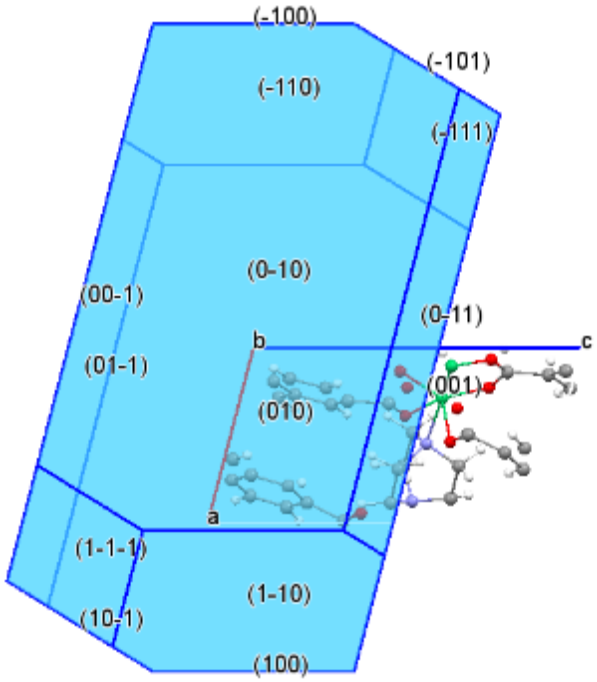

c)

DUT-8 (*op*)		DUT-8 (*cp*)	
Miller plane	BFDH Area	Miller plane	BFDH Area
100	0.160	001	0.207
-100	0.160	00-1	0.207
110	0.102	010	0.118
-1-10	0.102	0-10	0.118
1-10	0.102	-100	0.055
-110	0.102	100	0.055
00-1	0.071	10-1	0.050
001	0.071	-101	0.050
011	0.022	1-10	0.034
0-11	0.022	-110	0.034
0-1-1	0.022	0-11	0.018
01-1	0.022	01-1	0.018
-101	0.013	1-1-1	0.015
10-1	0.013	-111	0.015
0-20	0.001	-	-
020	0.001	-	-

Figure S1. BFDH morphologies for (a) DUT-8 (*op*) and (b) DUT-8 (*cp*) with (c) relative BFDH surface areas for each plane

Section S2. Creation of models to represent DUT-8 microcrystals and nanoparticles

Microcrystals have negligible external surface area to volume ratios; therefore, the influence of the external surface was neglected by implementing the bulk unit cell in periodic boundaries. As the particle size decreases, the surface area to volume ratio increases, so the external surface becomes more influential on the adsorption mechanism. Therefore, infinite slabs were used to model the surface effects in DUT-8 nanoparticles (**Figure S2**).

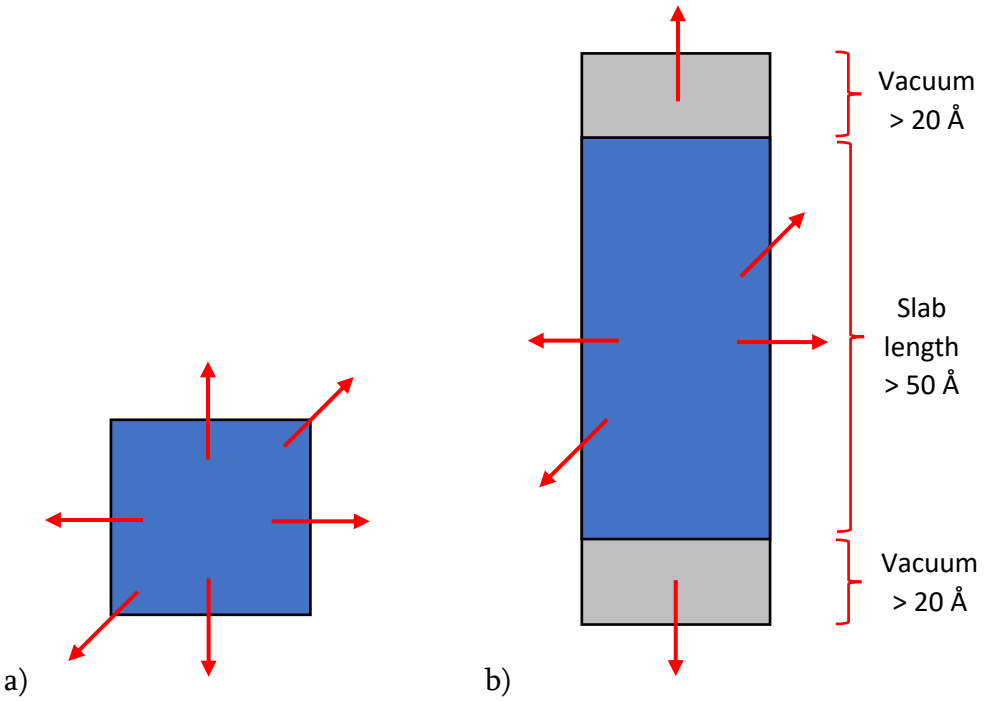

Figure S2. Schematic of (a) the bulk/microcrystal and (b) the slab/nanoparticle models. Red arrows indicate that periodic boundary conditions were applied in all three directions.

It was observed *via* face indexing single crystals that the (110) and (001) planes are most dominant, so slab models where cut with external faces along these planes. Coordination bonds between the nickel - nitrogen or nickel - oxygen atoms were cut, and uncoordinated metal sites were capped with either hydrogenated dabco, physisorbed DMF molecules, hydrogenated 2,6-ndc, or formate. These surfaces are shown in **Figure S3**.

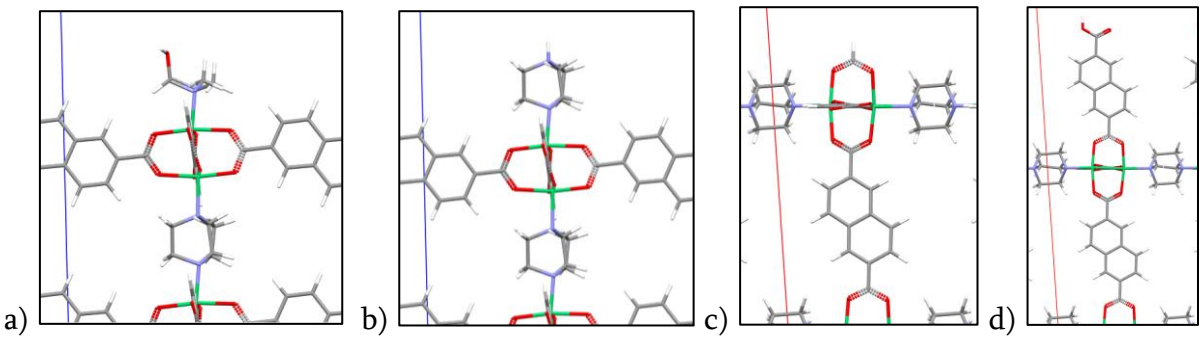

Figure S3. External surfaces of the slabs: (a) (001) DMF, (b) (001) dabco, (c) (110) formate, (d) (110) H(2,6-ndc).

Section S3. Isotherm normalization

Using the slab models results in inaccurate isotherms once the pores saturate due to extracrystalline adsorption in the vacuum gap leading to discrepancies between the experimental and simulated results. To account for this, a simple normalization can be applied to remove the influence of N_2 molecules in the vacuum gap: **Figure S4** shows the difference in isotherms when normalized.

Firstly, the difference in volume due to the vacuum gap needs to be accounted for by introducing a ratio, R, that scales the volume of the slab (V_{slab}) to the total volume of the slab unit cell (V_{total}). Since the volume of the slab is arbitrary, it is much easier to calculate *R* as a ratio of the density of the complete slab unit cell ($\rho_{slab_{UC}}$) to the density of the bulk crystal (ρ_{bulk}).

$$R = \frac{V_{slab}}{V_{total}} \approx \frac{\rho_{slab_{UC}}}{\rho_{bulk}}$$

Up to the point where extracrystalline adsorption occurs, the change in the excess amount adsorbed, Δn_{ex}, is equal to the change in the total amount adsorbed, Δn_{total}:

$$\Delta n_{ex} = \Delta n_{total}$$

When extracrystalline adsorption begins, the ratio is used to calculate the actual excess adsorption whilst removing the influence of the vacuum gap:

$$\Delta n_{ex} = R \cdot \Delta n_{total}$$

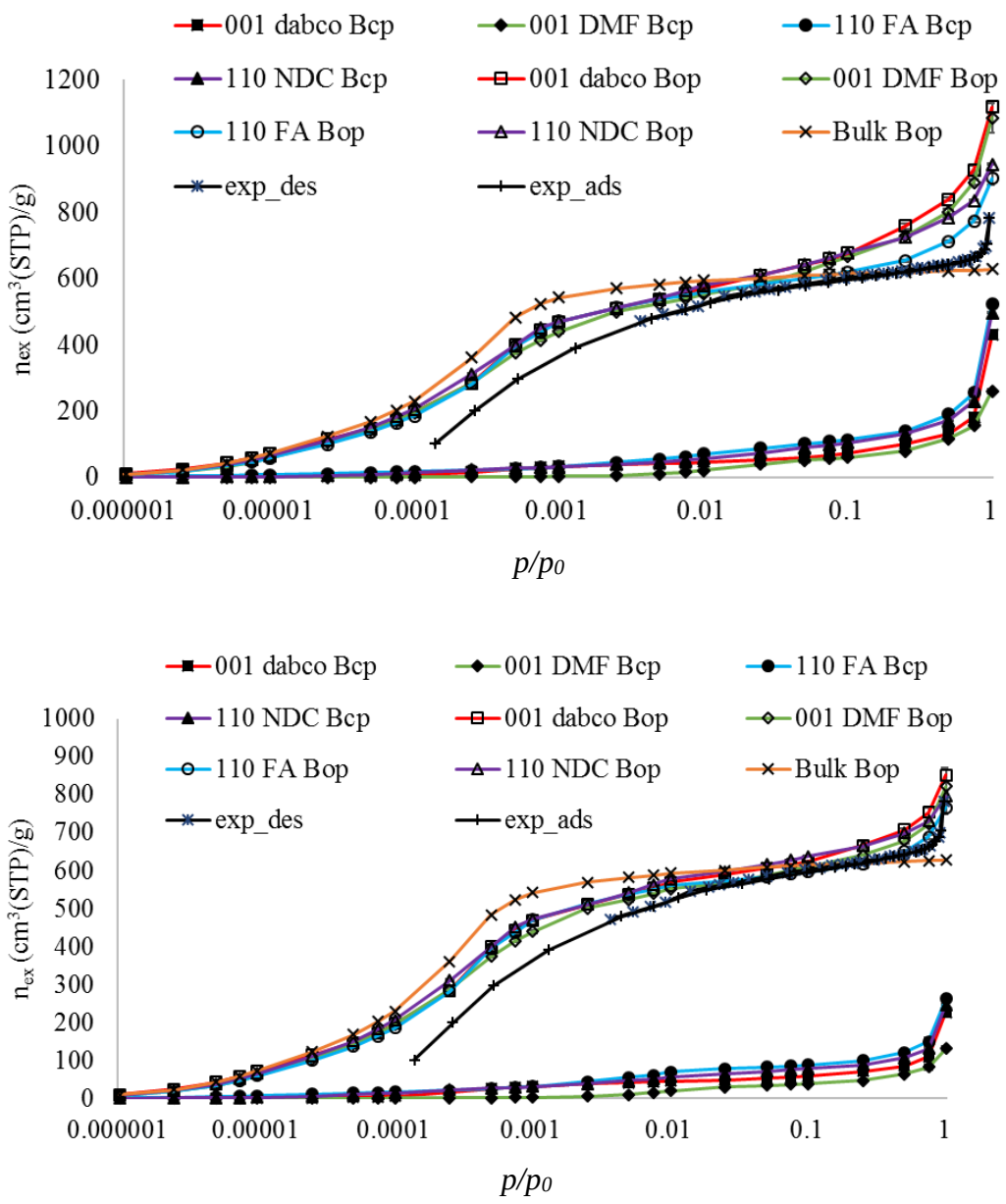

Figure S4: N_2 adsorption isotherms at 77 K in the slab models (and the experimental isotherm for comparison): a) original, and b) normalized to remove the influence of the vacuum gap.

Section S4. Phase transition prediction using osmotic framework adsorbed solution theory

To investigate the particle size dependence on phase transition, the osmotic framework adsorbed solution theory (OFAST) was used. In OFAST **Equation S1** is used to determine the osmotic potential Ω_k of the closed and open pore structures [4].

$$\Omega_k = F_k + PV_k - RT\int_0^P \frac{n_k}{P} dP \quad \text{S1}$$

Here, F_k is the free energy of the empty structure in phase k (kJ/UC), P is the total external pressure (kPa), V_k is the unit cell volume of the empty framework (m^3/UC), R is the ideal gas constant (0.008314 kJ/mol K), T is the temperature (77 K), and n_k is the moles of gas adsorbed in the unit cell (mol/UC). At the phase transition pressure, the osmotic potential of the closed and open pore structures should be equal, therefore at phase transition **Equation S2** holds true [4]:

$$\Delta F = \Delta\left(\Omega_i(P) - \Omega_i(P=0)\right) = RT\int_0^P \frac{\Delta n}{P} dP - P\Delta V \quad \text{S2}$$

A Langmuir type isotherm was fitted to the bulk/microcrystal GCMC results to calculate the integral: $n = \frac{M \cdot K \cdot P}{1+K \cdot P}\left(\frac{mol}{UC}\right)$. The integral can be evaluated using **Equation S3**:

$$-RT\int_0^P \frac{n_k}{P} dP = -RTMLN(1+KP) \quad \text{S3}$$

The nanoparticles do not exhibit Langmuir isotherms because of the extracrystalline adsorption at high pressures. For this reason, a correction was added to fit the high pressure region of the isotherm: $n = \frac{M \cdot K \cdot P}{1+K \cdot P} + \alpha P^2\left(\frac{mol}{UC}\right)$ (where α is a fitted variable).

Section S5. Characterisation of DUT-8(Ni) samples by PXRD.

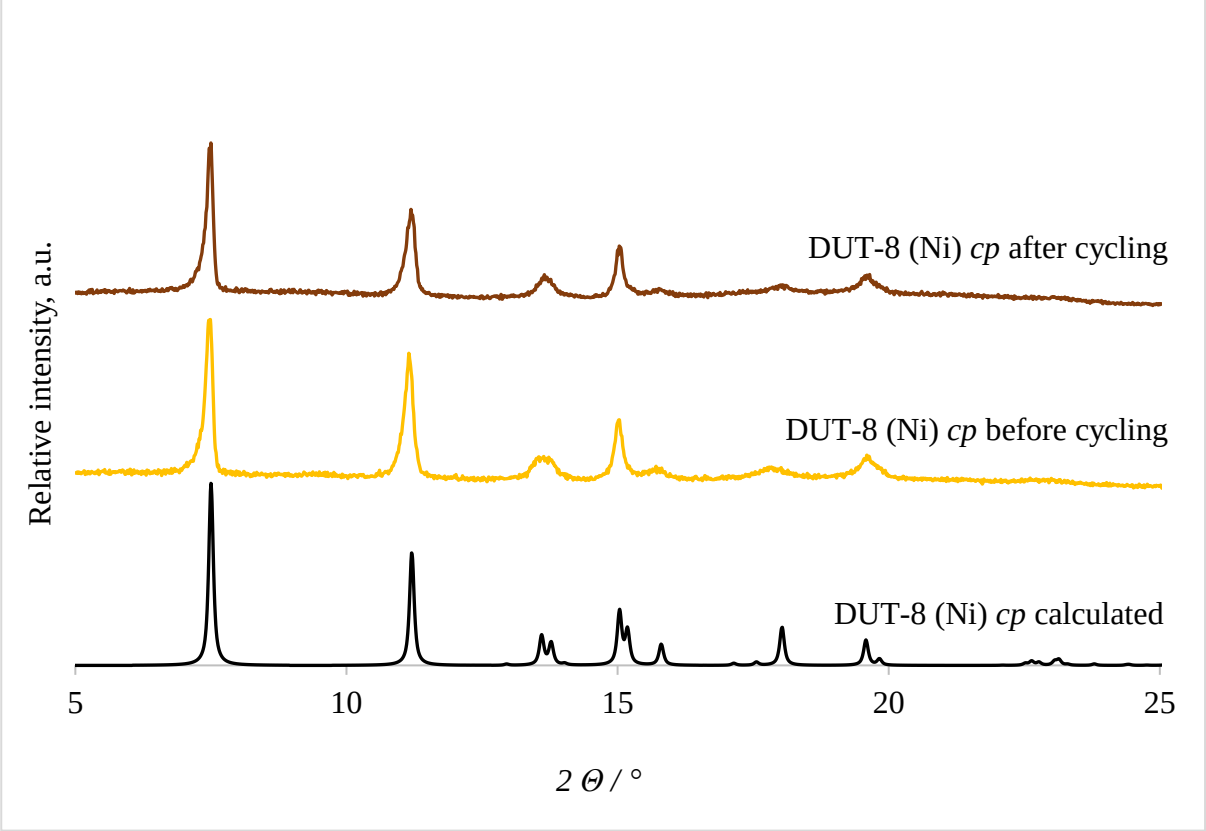

Figure S5. PXRD patterns for DUT-8(Ni): calculated for DUT-8(Ni) cp (black), activated sample before adsorption cyclization experiments (yellow), activated sample after 7 cycles of N_2/77K physisorption cycles (brown).

Section S6. Cyclic adsorption

Experimentally, cyclic adsorption of N_2 (amongst other guest molecules [5]) in the flexible DUT-8 microparticles causes their domain size to decrease, as shown in **Figure S6**. After seven cycles of N_2 adsorption at 77 K, the particle size decreases by over ten-fold, suggesting that the stress exerted on DUT-8(Ni) as it undergoes opening/closing causes the flexible crystals to undergo delamination.

a) 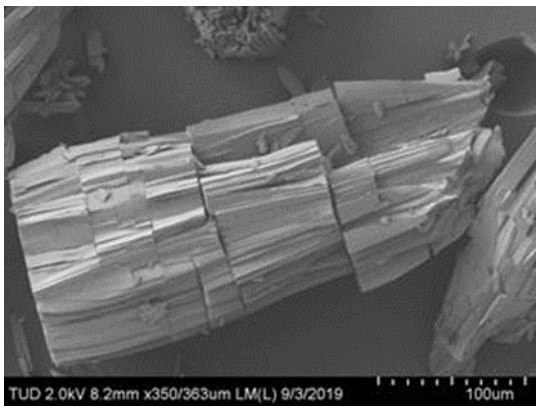

b) 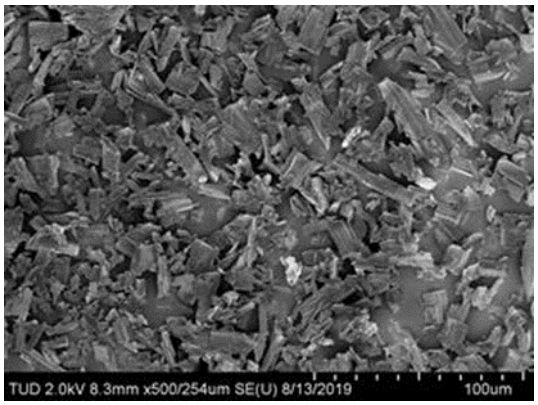

Figure S6 SEM images of flexible DUT-8(Ni) microparticles a) before and b) after seven cycles of N_2 adsorption at 77 K.

As the particle size decreases, the gate-opening/closing pressures increase because the cp structure becomes relatively more stable. **Figure S7** shows that after each cycle, there is a marginal decrease in the maximum uptake as well as in the slope of the isotherm. Such trends are indicative of weaker N_2 – DUT-8(Ni) interaction energies.

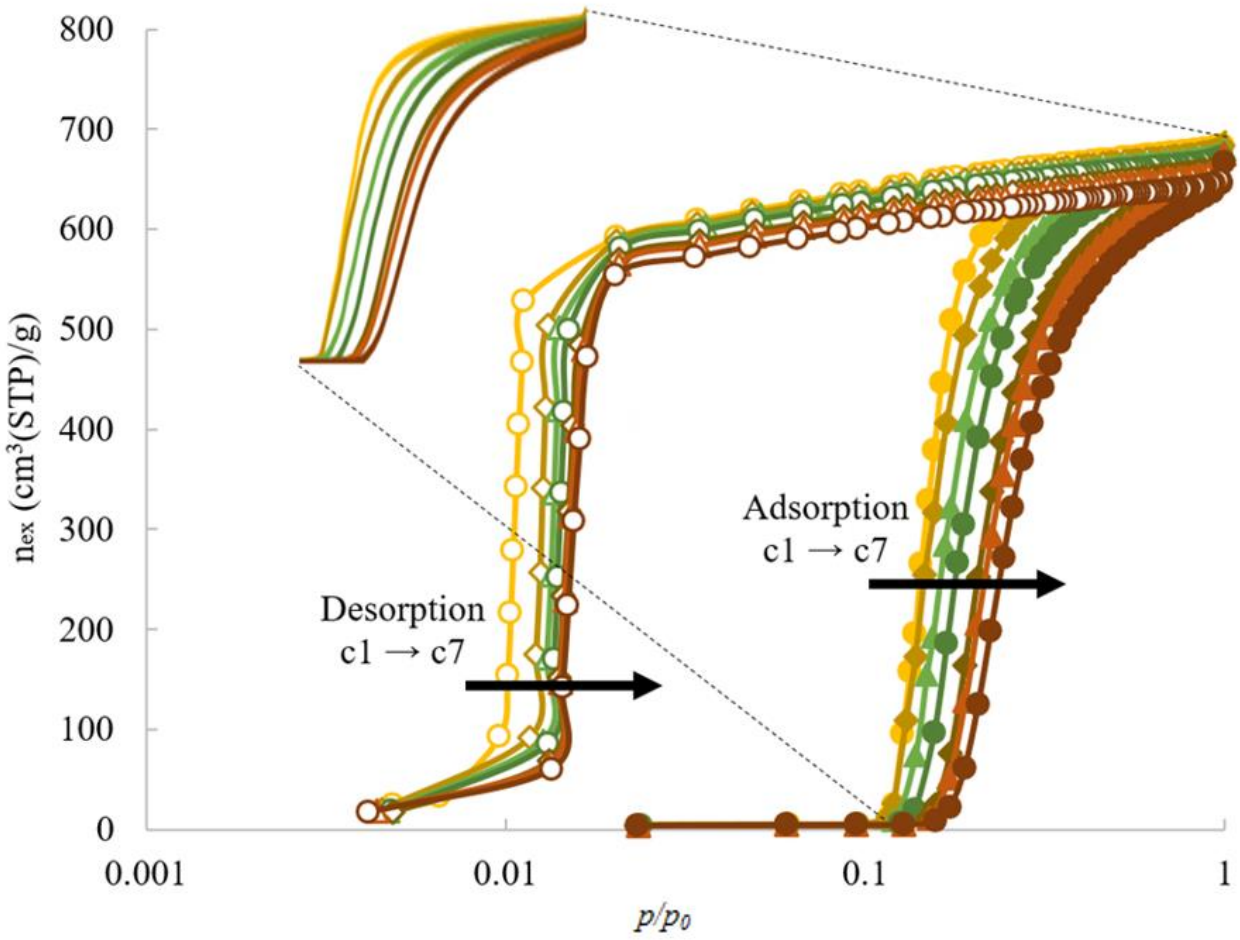

Figure S7. Experimental, cyclic adsorption of N_2 in the flexible microparticles at 77 K (showing seven cycles, c1 – c7)

Section S7. Boltzmann probability distributions

Figure S8 shows the Boltzmann probability distributions for N_2 adsorption in DUT-8, bulk conformer A*op* and B*op* at 77 K. There are no significant differences between the adsorption energy profiles in the two conformers

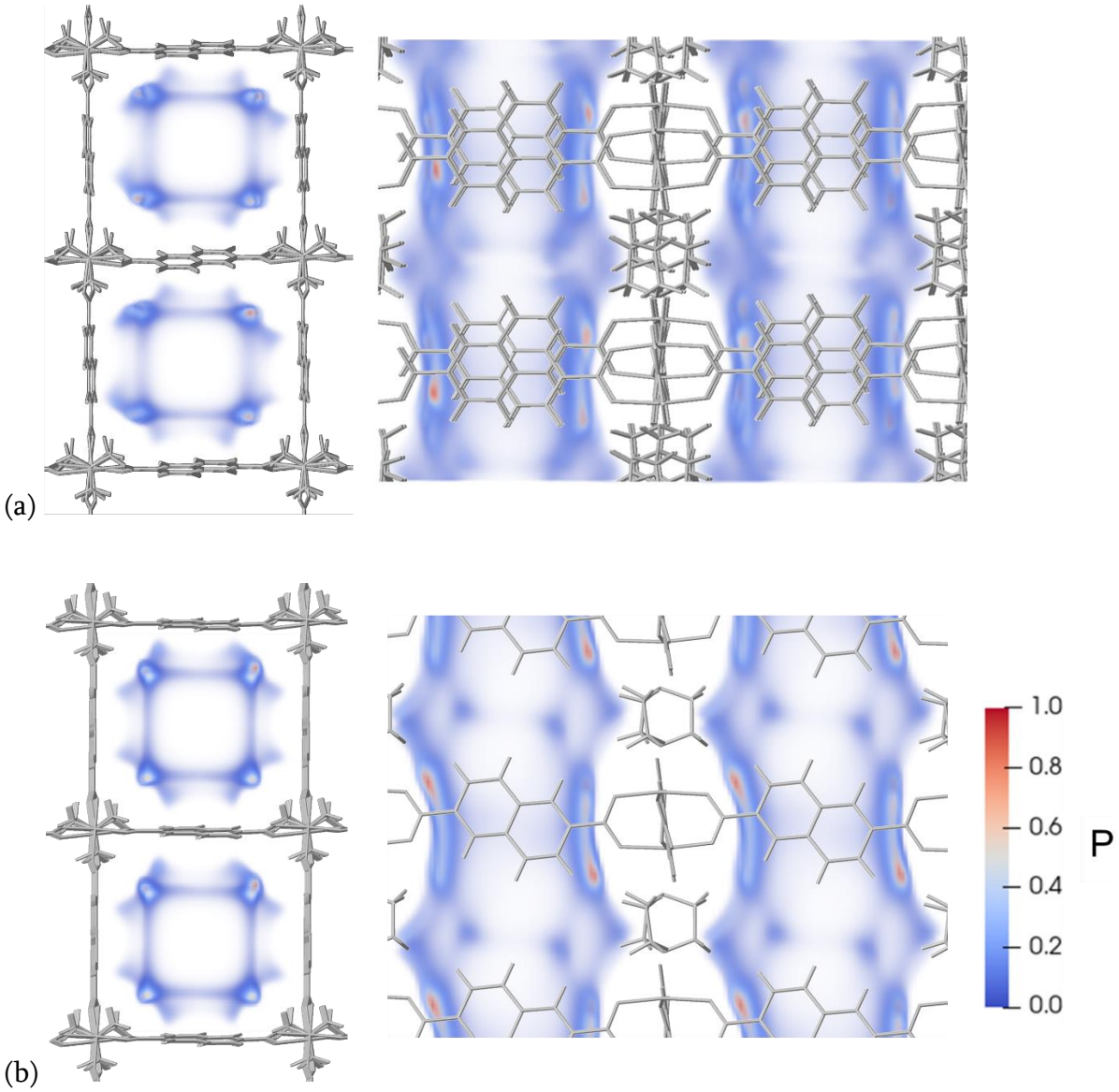

Figure S8. Boltzmann probability distribution for N_2 at 77 K inside the bulk conformer (a) A*op* and (b) B*op*.

Section S8. Why do the slabs models have a higher surface area to volume ratio than the experimental nanoparticles?

DUT-8(Ni) nanoparticles have a particle size of less than 500 nm. Assuming a spherical experimental nanoparticle of size equal to the thickness of the infinite slab models (i.e. 5 nm), the external surface area to volume ratio is:

$$\frac{4\pi\left(\frac{5}{2}\right)^2}{\frac{4}{3}\pi\left(\frac{5}{2}\right)^3} = 1.2\ \mathrm{nm}^2/\mathrm{nm}^3$$

Considering the cuboidal slabs, the external surface area to volume ratio is approximately:

$$\frac{2(2\times 2)}{2\times 2\times 5} = 2.5\ \mathrm{nm}^2/\mathrm{nm}^3$$

Increasing the size of the real-life spherical nanoparticles decreases the external surface area to volume ratio since the surface area scales with r^2, whereas the volume scales with r^3. Therefore, the slabs always have a larger external surface area to volume ratio compared to the experimental crystals.

Section S9. OFAST gate-closing prediction for the bulk

Ab-initio minimisations were used to calculate the internal energy differences of the empty frameworks. **Figure S9** shows that A*op* and B*op* have similar internal energies ($\Delta E_{Aop-Bop} = 6$ kJ mol^{-1}). The strain penalty associated with closing conformer A is greater than the change in dispersion interactions, and so A*op* cannot spontaneously close into A*cp* ($\Delta E_{Aop-Acp} = 37$ kJ mol^{-1}). B*cp* is more favourable than either *op* structure as the dispersion

interactions dominate. The calculated energy difference between the conformer B structures ($\Delta E_{Bcp-Bop} = -76$ kJ mol^{-1}); is slightly smaller than the energy difference calculated by Petkov et al, ($\Delta E_{Bcp-Bop} = -102$ kJ mol^{-1}), who used different pseudopotentials and basis sets [6]). Both sets of results however are consistent with the experimental observation that "as-made" microparticles revert to B*cp* upon solvent removal [3, 7].

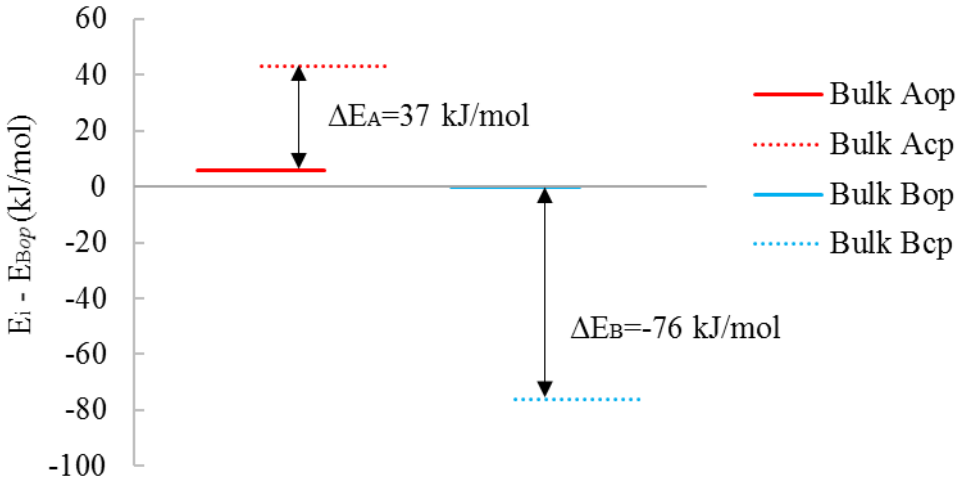

Figure S9: Relative internal energies of the empty bulk crystals

Figure S10 shows that the relative osmotic potentials of the conformer B structures overlap at a nitrogen pressure of $p/p_0 = 0.005$. This is the pressure at which the N_2-DUT-8 systems are in equilibrium (i.e. the gate-closing pressure) [4]. Regardless of the pressure, Ω_{Aop} is always more favourable than Ω_{Acp}, and so the A*op* conformer of DUT-8 cannot transform into the A*cp* isomer.

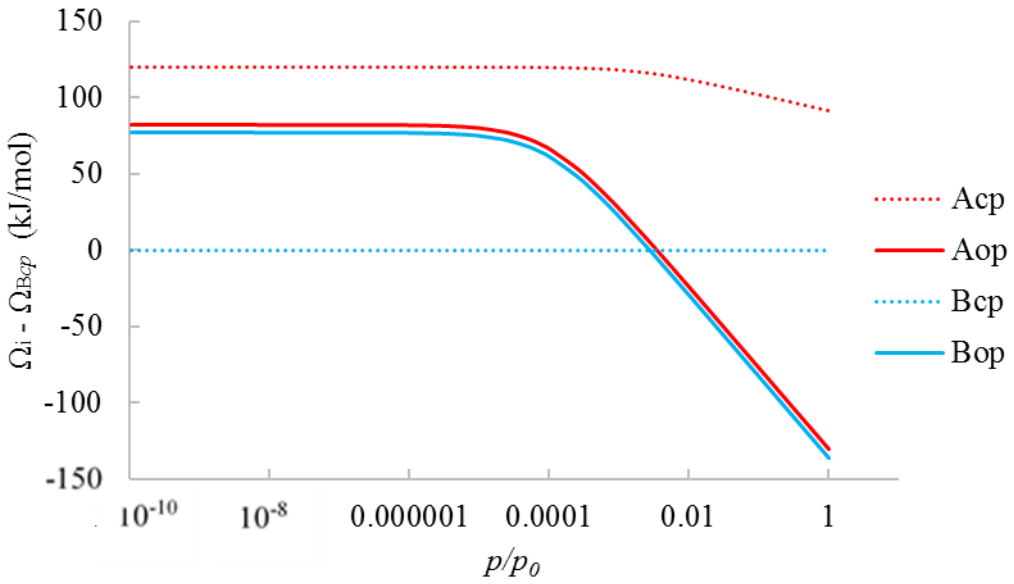

Figure S10: Relative osmotic potentials for N_2 adsorption at 77 K in the bulk framework

Section S10. Energy difference and gate closing pressures for different capping groups

OFAST was used to predict the gate-closing pressure in the bulk and slab models. **Table S1** shows the internal energy differences and the gate-closing pressure for each system.

Table S1. Normalized (solvent free) B*cp* → B*op* energy differences and the gate closing pressures for each capping group

System	$E_{Bop\text{-}Bcp}$/Bulk (kJ/mol)	$p/p^{o^{closing}}$
001-DMF	33	0.003
110-FA	53	0.01
001-dabco	59	0.03
110-H(2,6-ndc)	69	0.05
Bulk	76	0.005

REFERENCES

1. Macrae, C.E., P; McCabe, P; Pidcock, E; Shields, G; Taylor, R; Towler, M; van de Streek, J, *Mercury.* Journal of Chemical Information and Modeling, 2006. **44**: p. 2133-2144.
2. Donnay, J.H., D, *A new law of crystal morphology extending the law of Bravais.* American Mineralogist, 1937. **22**(463): p. 446-467.
3. Bon, V., et al., *Exceptional adsorption-induced cluster and network deformation in the flexible metal–organic framework DUT-8(Ni) observed by in situ X-ray diffraction and EXAFS.* Physical Chemistry Chemical Physics, 2015. **17**(26): p. 17471-17479.
4. Coudert, F.-X., *The osmotic framework adsorbed solution theory: predicting mixture coadsorption in flexible nanoporous materials.* Physical Chemistry Chemical Physics, 2010. **12**(36): p. 10904-10913.
5. Bon, V., et al., *Tolerance of Flexible MOFs toward Repeated Adsorption Stress.* ACS Applied Materials & Interfaces, 2015. **7**(40): p. 22292-22300.
6. Petkov, P., et al., *Conformational isomerism controls collective flexibility in metal-organic framework DUT-8(Ni).* Physical Chemistry Chemical Physics, 2018.
7. Klein, N., et al., *Monitoring adsorption-induced switching by (129)Xe NMR spectroscopy in a new metal-organic framework Ni(2)(2,6-ndc)(2)(dabco).* Phys Chem Chem Phys, 2010. **12**(37): p. 11778-84.